LNF-96/025

Microstructure and Phase Morphology of Diamond Thin Films by Synchrotron Radiation X-Ray Diffraction

G. Cappuccio, M. Leoni, P. Scardi, V. Sessa, M. L. Terranova

Materials Science Forum 203, 285-289, (1996)

Materials Science Forum Vol. 203 (1996) pp. 285-290

Microstructure and Phase Morphology of Diamond Thin Films by Synchrotron Radiation X-Ray Diffraction

G. Cappuccio[1], M. Leoni[2], P. Scardi[2], V. Sessa[3] and M.L. Terranova[3]

[1] CNR, Ist. Strutturistica Chimica, PO Box 10, I-00016 Monterotondo, Italy
and INFN - LNF - Lab. Raggi X POB 13, I-00044 Frascati, Italy

[2] Università di Trento, Dipartimento di Ingegneria dei Materiali, I-38050 Mesiano, Italy

[3] Università di Tor Vergata, Dipartimento di Scienze e Tecnologie Chimiche,
Via della Ricerca Scientifica, I-00133 Roma, Italy

Keywords: CVD, Diamond, Microstrain, Grain-Size, Synchrotron Radiation, X-Ray Diffraction, Grazing Incidence Diffraction

Abstract

Diamond films grown on titanium substrates by hot filament chemical vapour deposition (HF-CVD) were characterised by X-ray diffraction (XRD) measurements using both synchrotron radiation (SR) and a Cu X-ray tube. Grazing incidence diffraction (GID) measurements pointed out the presence of different phases at the film-substrate interface, i.e. titanium hydride (TiH_2) and titanium carbide (TiC). The experimental data allowed us to determine, by means of a line broadening analysis (LBA), the crystallographic features and microstrain of the diamond layer and of the other phases.

Introduction

During the growth of polycrystalline diamond thin-films on titanium substrates, using the hot filament CVD method, titanium-hydride (TiH_2) and titanium-carbide (TiC) are formed at the substrate-film interface. The presence of such phases gives rise to stress-strain effects, due to the mismatch between the different lattice parameters, which influence the mechanical stability of the diamond coating. In order to clarify film structure and lattice disorder, X-ray diffraction measurements were recently performed with the synchrotron radiation Station 2.3 at Daresbury (UK). X-ray grazing incidence diffraction measurements have shown the growing sequence of the different phases and have allowed a rough estimation of the different layer thicknesses. Taking advantage of the high resolution, intensity and monochromaticity of SR, a line broadening analysis (LBA) was performed on Bragg reflections from the various phases, in order to calculate crystallite mean size and microstrain.

Experimental

The diamond films were obtained using the hot filament CVD technique, with a reactant mixture of 1% CH_4/H_2 activated by a tantalum filament kept at 2180 °C [1]. Typical deposition parameters were: pressure 36 Torr, gas flow rate 200 sccm, and substrate temperature 650 °C.

X-ray diffraction (XRD) experiments were conducted at the synchrotron radiation source (SRS) of Daresbury Laboratory (U.K.). Station 2.3 was equipped with a double crystal monochromator in the incident beam for wavelength selection, and a two-circle goniometer with a customised rotating holder for small samples. A vertical 1.3 slit and a horizontal 10 mm slit were used to limit the beam within the sample surface, whereas a long Soller slit in the scintillation counter arm was used to produce narrow profiles and reduce errors in peak position [2].

All the XRD measurements were done in the θ-2θ traditional mode, selecting λ=1.5406 Å. After goniometer calibration by a Si standard powder (NBS 640b), thin film measurements were carried out using 0.05° step and 4 sec counting time. For a reliable line broadening analysis (LBA), the instrumental function was measured by a KCl standard powder [3] in the range 2θ=28°÷120°.

The same instrumental configuration, but with narrower vertical slits, was used for grazing incidence diffraction measurements, in order to compare their results with analogous measurements made in laboratory using a Bragg-Brentano diffractometer with a Cu X-ray tube. The sample was

kept at a pre-fixed θ angle (0.5°, 1°, 2°,...), while the scans were performed in the range 2θ = 34°÷46°.

Grazing Incidence and Line Broadening Analysis

The XRD measurements demonstrated the presence of four phases, while the GID measurements showed their growth sequence, i.e., starting from the top-most layer: diamond, TiC, TiH_2 and the α-Ti matrix (cf.Fig.1).

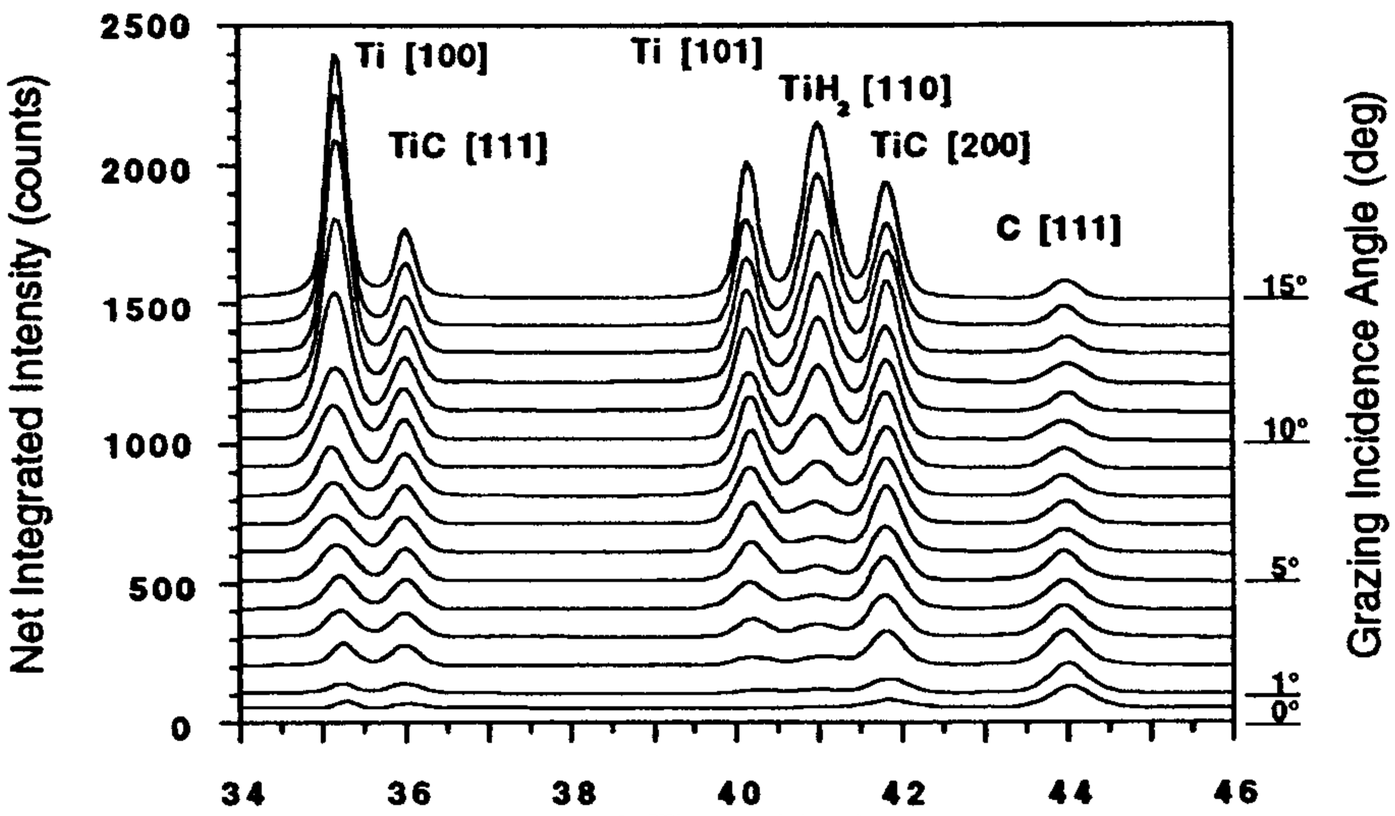

Figure 1. The stratification sequence of the different phases shown by the X-ray grazing incidence diffraction measurements for the 270 min-grown sample.

The presence of these four phases caused remarkable peak overlapping problems; and the need to use analytical profile modelling can be appreciated in Fig. 2, which shows both experimental and modelled patterns along with their differences. The results of profile fitting of Bragg-Brentano diffraction patterns were used as input for the line broadening analysis.

Owing to the lack of measurable second-order reflections, traditional methods such as that of Warren-Averbach (WA) [4-7] could not be used. To overcome these limitations, the following procedure was adopted: (i) the XRD pattern was modelled by a non-linear least-squares routine, employing pseudo-Voigt (pV) functions for Bragg's peaks and a straight line for background [8-10]; (ii) the same procedure was followed for a KCl profile standard sample [3]; thus the instrumental function was parametrized, as shown in Fig. 3, and the correction of measured profiles for the instrumental broadening could be performed analytically; (iii) a single-line (SL) procedure for LBA was carried out with a method originally proposed by Nandi et al. [11], and only briefly reviewed here. The interested reader can refer to the cited literature for details [11,12].

Starting from the cosine Fourier coefficients of a Bragg's peak A_n, (corrected for the instrumental broadening (ii)), it was demonstrated that [7]:

$$A_n = A_n^S \cdot A_n^D \tag{1}$$

where n is the harmonic number, A_n^S, A_n^D are the broadening components due to size effect and lattice distortion, respectively. Taking advantage of the fact that only the distortion component depends on the diffraction order, the WA method permits the separation of size and distortion effects when at least two peaks of the same crystallographic family are known (e.g., (111) and (222)). In particular, it can be shown that :

$$A_L^D = 1 - \left(2\pi^2 \cdot m^2 \cdot \langle \varepsilon^2(L) \rangle \cdot L^2 / d_{hkl}^2\right) \tag{2}$$

where m is the diffraction order and $\langle \varepsilon^2(L) \rangle^{1/2}$ is the microstrain; L is the distance between cells

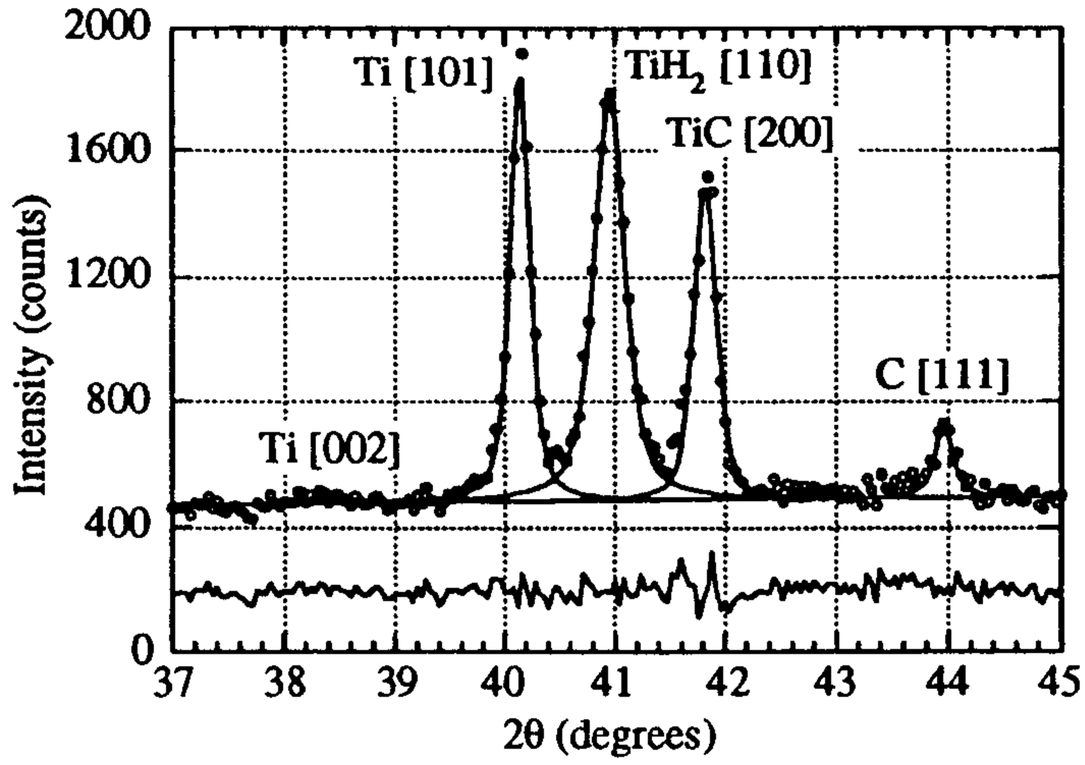

Figure 2. Experimental and modelled pattern of the 270 min-grown sample. The residual (difference between experimental and modelled) is reported below the figure.

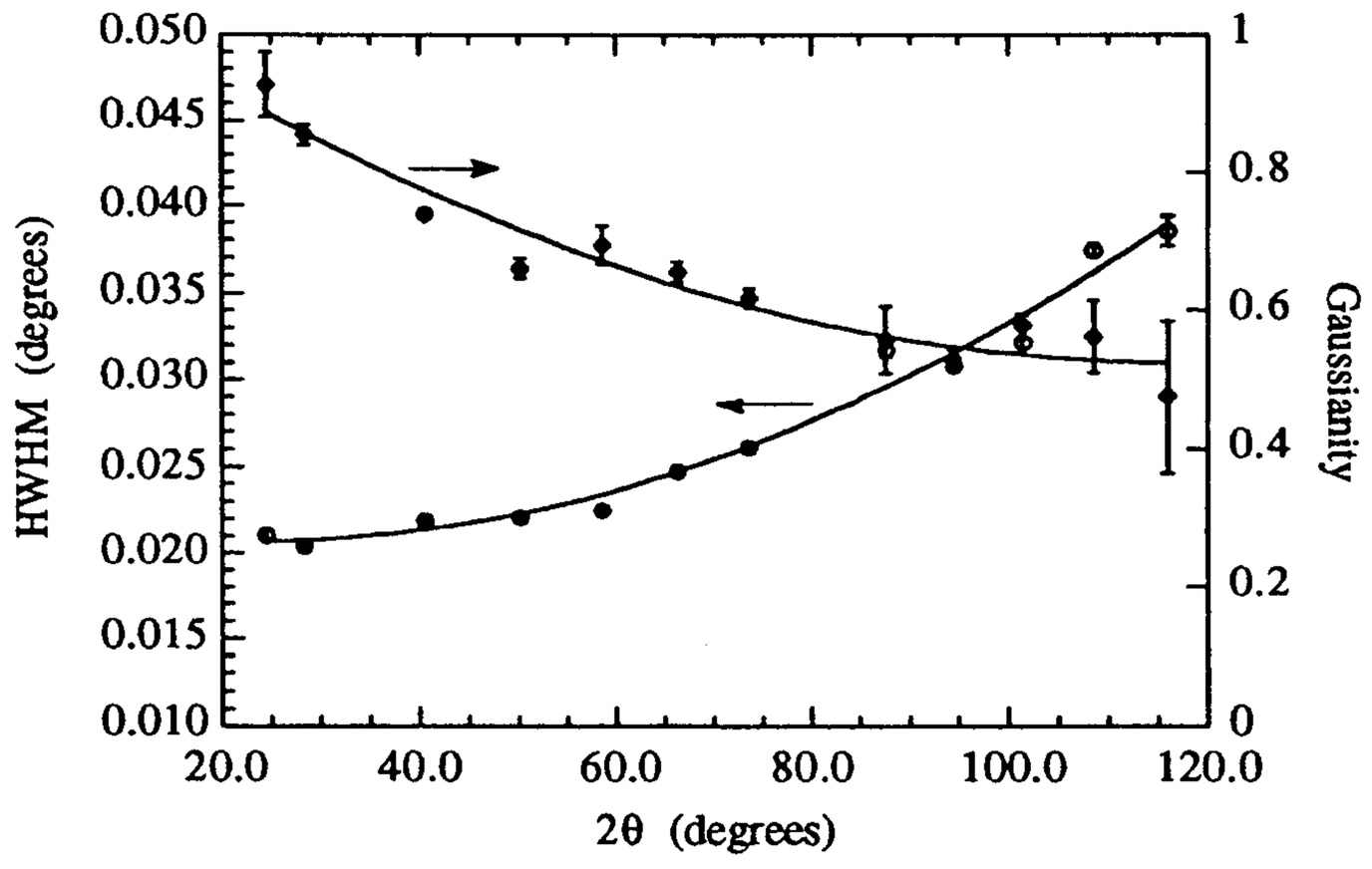

Figure 3. Half width at half maximum and Gaussianity of the pV functions used to model the instrumental profile of station 2.3.

n-times apart along [hkl], namely $L = n \cdot d_{hkl}$, where d_{hkl} is the interplanar distance.

When only a single line is known, many approximated methods have been proposed [7-13]. In the present work we applied the method proposed by Nandi et al. [11] because it is particularly reliable with regard to crystallite size values [11-14] and can be easily adapted for use with analytically modelled profiles. The method assumes that the size component A_L^S has a trend which can be described by an exponential function:

$$A_L^S \cong \exp\left(-L/\overline{M}\right) \tag{3}$$

where $\overline{M}$ is the mean column length along [hkl] and can be obtained through an approximation, from the initial slope of the A_L vs. L plot:

$$\lim_{L\to 0} A_L \cong 1 - L/\overline{M} \tag{4}$$

The microstrain can be calculated from Eqs. (2-4); in fact, for a cubic lattice, considering $A_{M/2}$ (the Fourier coefficient at $L=\overline{M}/2$):

$$< \varepsilon^2 >_{M/2}^{1/2} = \left\{ \left[1 - \frac{A_{M/2}}{e^{-1/2}} \right] \cdot 2d_{hkl}^2 \Big/ \pi^2 \cdot m^2 \cdot \overline{M}^2 \right\}^{1/2} \tag{5}$$

The choice of $L=\overline{M}/2$ to evaluate the microstrain is arbitrary, although it is frequently assumed as a representative value to evaluate lattice disorder when working with Fourier coefficients of a reasonable magnitude ($A_{M/2} \approx 0.5$).

Results and Discussion

The three samples considered in the present study differed from each other in deposition time, which changed the diamond thickness and also influenced the microstructure.

The results of the profile fitting of Bragg-Brentano diffraction patterns (Fig. 2) were used as input for LBA, following the SL procedure described above. As for the diamond, only the (220) and the weak (111) reflections were visible in the X-ray pattern thus, only two reflections along different crystallographic directions were considered for the interfacial compounds: TiH_2 (110), (200); TiC (200), (220). Figure 4 shows the trend of $\overline{M}$ and $< \varepsilon^2 >_{M/2}^{1/2}$ for TiC, TiH_2 and diamond. Given their isotropy, average values are reported for TiC and TiH_2, whereas $\overline{M}$ and $< \varepsilon^2 >_{M/2}^{1/2}$ along [111] and [220] are considered for diamond. As shown in the Figure 4, crystallite size and microstrain in TiC and TiH_2 do not vary considerably along the different directions. The diamond crystallites are much longer, and conseguently the microstrain much lower, along [220] than along [111]. TiC and TiH_2 showed crystallite sizes ranging between 15 and 25 nm, while diamond crystallites were considerably anisotropic: 15 and 50 nm along the [111] and [220] directions, respectively.

From the figure, it can be seen that for longer deposition times, TiH_2 crystallites tend to be smaller than those of TiC. Conversely, diamond is clearly subjected to a progressive grain growth, going from 45 nm for 180' to 76 nm for 270'. Note that $< \varepsilon^2 >_{M/2}^{1/2}$ is very low along [220], at the limit of sensitivity of LBA, whereas it is much higher along [111] and tends to decrease with increasing time.

These results are in agreement with the trend exhibited by the net integrated intensity ratio [220]/[111], which increases with deposition time [15]. Therefore, longer deposition leads to a better crystallisation of diamond, even though it does not eliminate the small fraction of [111] grains. This is understandable if we consider the particular phase growth mechanisms. The two Ti compounds grew at the film/substrate interface, due to interstitial diffusion of carbon and hydrogen inside the α-Ti matrix. Since their growth direction is strongly dependent on the original texture of the substrate, it is logical that both TiC and TiH2 grains are randomly oriented.

On the contrary, diamond crystallites are considerably anisotropic. A preferential orientation of the diamond crystallites towards the <hh0> direction is found to develop during the deposition process. As a consequence, the grains tend to be columnar along the main growth direction, as typical of many thin film systems, especially epitaxial thin films [16-18].

Conclusions

The findings of the present investigation demonstrate that the combined use of different diffraction techniques, i.e. XRD and GID represents a powerful tool for characterising layered structure grown during the CVD synthesis of diamond. In particular, these techniques allowed us to define microstrain, connected with the lattice disorder, and grain size of the different phases. It was also possible to study the growth kinetics and demonstrate the position sequence of TiC and TiH_2. Further analyses of data, collected by means of synchrotron radiation, are in progress in order to evaluate the strain values.

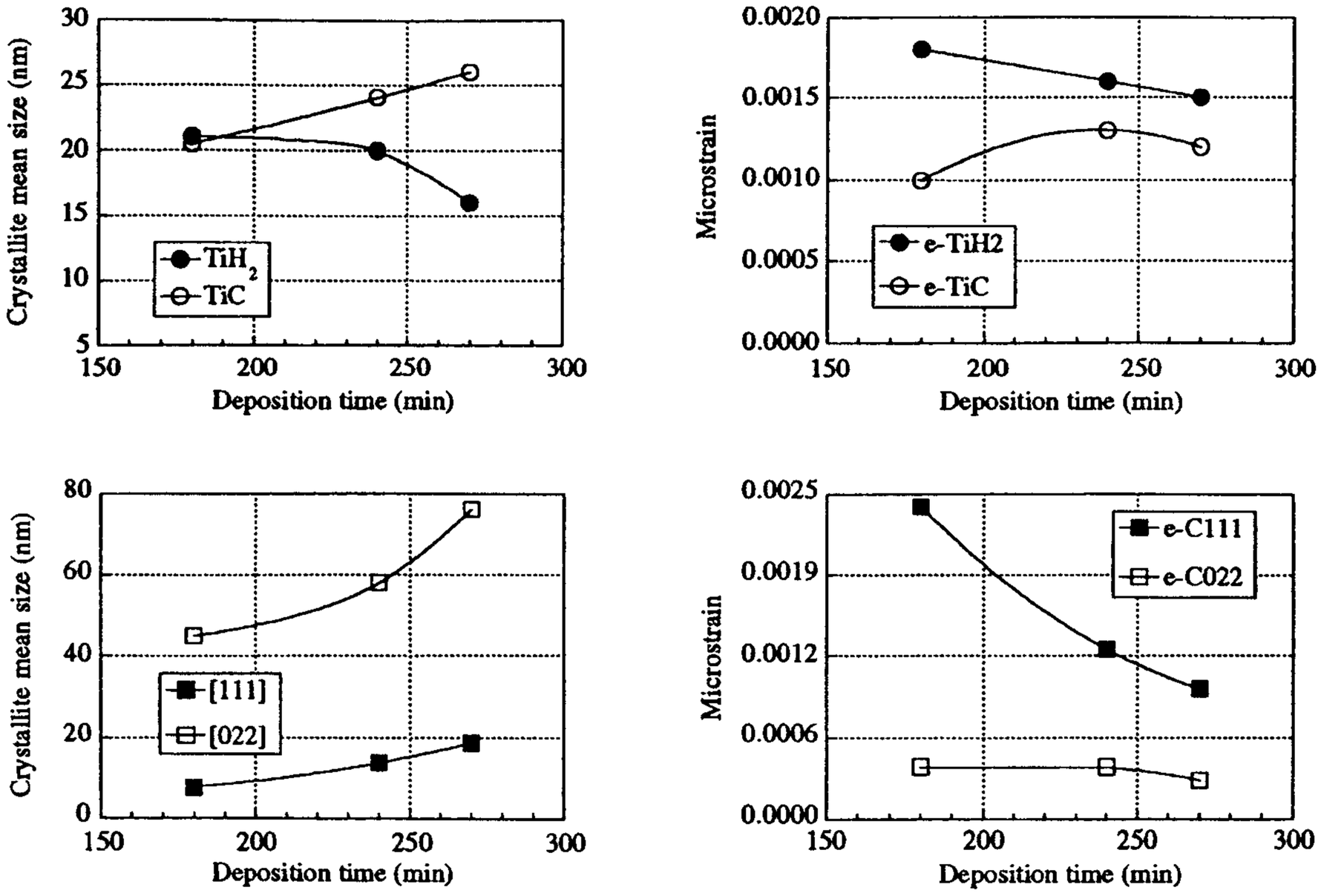

Figure 4. Crystallite mean size and microstrain as a function of the deposition time. Average values are shown for TiC and TiH_2; for diamond the values are given along the [111] and [022] directions.

References

[1] M. L. Terranova, R. Polini, V. Sessa, M. Braglia and G. Cocito, Diamond Rel. Mater. **1**, 969 (1992).
[2] R.J. Cernik, P.K. Murray, P. Pattison and A.N.Fitch, J. Appl. Cryst. **23**, 292 (1990) .
[3] P. Scardi, L. Lutterotti and P. Maistrelli, Powder Diffraction **9**, 180 (1994).
[4] B.E. Warren and B.L. Averbach J. Appl. Phys. **21**, 595 (1950).
[5] B.E. Warren and B.L. Averbach J. Appl. Phys. **23**, 1059 (1952).
[6] B.E. Warren, "X-ray Diffraction" (Addison-Wesley, Reading, MA, 1969), pp.251-314.
[7] H.P. Klug and L.E. Alexander, "X-ray Diffraction Procedures for Polycrystalline and Amorphous Materials" (Wiley, New York, 1974), 2nd ed., pp 642-708
[8] S. Enzo, G. Fagherazzi A. Benedetti and S. Polizzi, J. Appl. Cryst. **21**, 536 (1988).
[9] A. Benedetti, G. Fagherazzi S. Enzo and M. Battagliarin, J. Appl. Cryst. **21**, 543 (1988).
[10] P. Scardi, L. Lutterotti, R. Di Maggio, Powder Diffraction **6**, 20 (1991).
[11] R.K. Nandi, H.K. Kuo, W. Schlosberg, G. Wissler, J.B. Cohen and B. Crist Jr, J. Appl. Cryst. **17**, 22 (1984).
[12] Th.H. de Keijser, J.I. Langford, E.J. Mittemeijer and A.B.P. VogelsJ. Appl. Cryst. **15**, 308 (1982).
[13] D. Balzar, J. Appl. Cryst. **25**, 559 (1992).
[14] D.C. Kothari, P. Scardi, S. Gialanella and S. Guzman, Philos. Mag., **61**, 627 (1990).
[15] G. Cappuccio, V. Sessa, M.L. Terranova and C. Veroli, Materials Science Forum **166-169**, 325 (1994)
[16] P. Scardi, D.C. Kothari, L. Guzman, Thin Solid Films, **195**, 213 (1991).
[17] P. Scardi, L. Lutterotti, L. Correra and S. Nicoletti, J. Mat. Res. **8**, 2780 (1993).
[18] P. Scardi, in Science & Technology of Thin Films, ed. F.C. Matacotta and G. Ottaviani (World Scientific publisher, 1995). In press.